Geophysical Research Letters

Key Points:
- Regional finite element ice-flow modeling was used to investigate the drivers and controls of kilometer-scale, Holocene ice sheet retreat
- Topographic pinning points controlled the rate of ice loss during retreat until a threshold was reached, after which retreat was rapid
- Enhanced ocean-driven melt in the Early-to-Mid Holocene explains the timing of the rapid ice loss in this region

Supporting Information:
- Supporting Information S1

Correspondence to:
R. S. Jones,
richard.s.jones@monash.edu

Ocean-Driven and Topography-Controlled Nonlinear Glacier Retreat During the Holocene: Southwestern Ross Sea, Antarctica

R. S. Jones[1,2] , G. H. Gudmundsson[3] , A. N. Mackintosh[1] , F. S. McCormack[1] , and R. J. Whitmore[1]

[1]School of Earth, Atmosphere and Environment, Monash University, Melbourne, VIC, Australia, [2]Science Laboratories, Department of Geography, Durham University, Durham, UK, [3]Geography and Environmental Sciences, Northumbria University, Newcastle upon Tyne, UK

Abstract Recent ice sheet mass loss in Antarctica has been attributed to an influx of warm ocean waters, which drove grounding-line retreat and ice thinning. Episodic retreat and rapid thinning also occurred in the southwestern Ross Sea during the Holocene, which today accommodates cold ocean waters. We applied finite element ice-flow modeling to investigate the roles of ocean temperature and bed topography in the deglaciation of this region. First, our experiments demonstrate that bed topography controlled the spatial pattern of grounding-line retreat. Topographic pinning points limited the rate of ice loss until retreat progressed beyond a bathymetric threshold. Second, ocean thermal forcing determined the timing of this ice loss. Enhanced ocean-driven melt is required during the Early-to-Mid Holocene to replicate geological records of deglaciation, possibly indicating that warm ocean waters were once present in this region. On multi-centennial timescales, ocean temperature drove, while bed topography controlled, nonlinear rates of ice mass loss.

Plain Language Summary Parts of the Antarctic Ice Sheet are currently losing mass at an accelerating rate. The main cause is considered to be warming ocean waters, which melt the underside of floating ice shelves, initiating retreat and inland thinning of the ice sheet. Future ice loss will depend on when and where ocean warming occurs, and how the ice sheet responds. However, modern observations are too short to fully assess the effects of these processes. We use a state-of-the-art numerical ice-flow model to investigate the roles of ocean warming and bedrock geometry during a period of accelerated ice sheet thinning in the recent geological past. We find that seafloor mounts and banks helped to slow down the rate of ice sheet retreat. Once the grounded ice became detached from these parts of the bedrock, retreat accelerated across areas of deeper water, causing rapid inland thinning of the ice sheet. Crucially, we also find that this period of past rapid thinning was initiated by an enhanced rate of ocean warming. This work highlights that key processes governing modern and future ice sheet mass loss— ocean warming and feedbacks associated with bedrock geometry—occurred in the past on timescales of centuries to millennia.

1. Introduction

The Antarctic Ice Sheet has been losing mass at an accelerating rate over recent decades (Rignot et al., 2019; Shepherd et al., 2018), coincident with grounding-line retreat and associated inland thinning (Konrad et al., 2018; McMillan et al., 2014). The primary cause of this ice loss is considered to be the thinning of ice shelves by ocean-driven basal melt (Gudmundsson et al., 2019; Rignot et al., 2013; Smith et al., 2020). Future ice loss beyond this century will likely occur from a combination of thinning ice shelves and topographic feedbacks as grounding lines retreat into basins that lie below sea level (DeConto & Pollard, 2016; Golledge et al., 2015; Meredith et al., 2019). Despite an improved capability of models to simulate the processes controlling retreat, significant discrepancies in projections remain (Oppenheimer et al., 2019). A better understanding of the drivers and controls of future centennial-scale ice loss can be obtained by investigating deglaciation in the geological past.

A combination of forcings drove changes in the Antarctic Ice Sheet over glacial-interglacial cycles (Noble et al., 2020; Tigchelaar et al., 2019), but ocean thermal forcing was likely the main driver of Antarctic ice
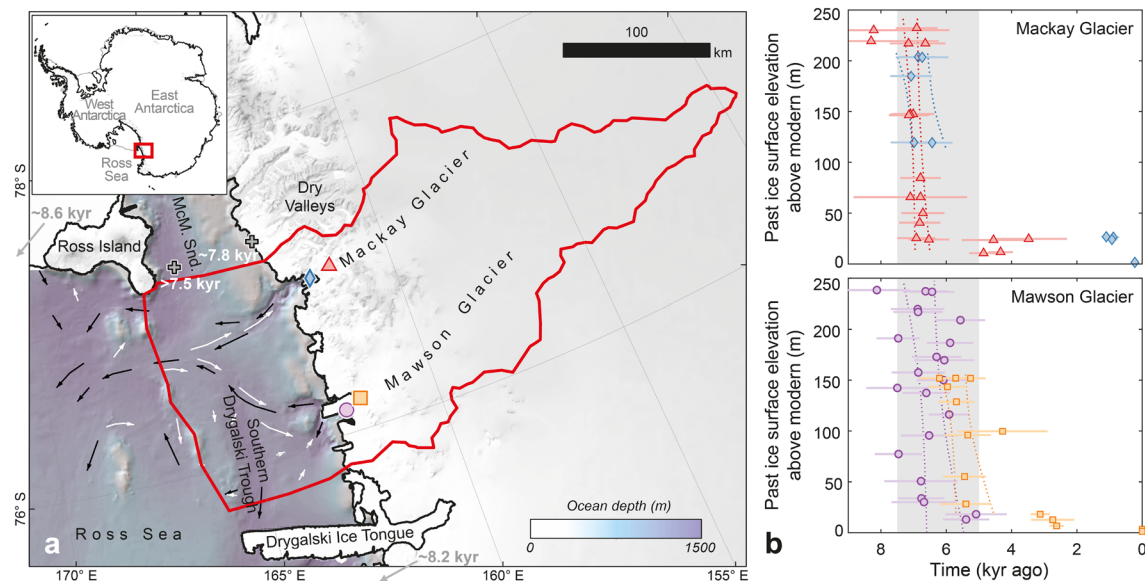
Figure 1. (a) Study region, showing the present-day ice surface (Howat et al., 2019) and offshore bathymetry (Arndt et al., 2013; Lee et al., 2017). Black and white arrows represent the proposed directions of ice flow and grounding-line retreat during the Holocene based on the interpretation of seafloor landforms (Greenwood et al., 2018; Lee et al., 2017). The timing of deglaciation is partly constrained in the McMurdo Sound (McM. Snd.) (gray crosses; Hall & Denton, 2004; Licht et al., 1996), as well as east of Ross Island and north of the Drygalski Ice Tongue in Terra Nova Bay (Baroni & Hall, 2004; McKay et al., 2016). Onshore, ice thinning is recorded at Mackay Glacier (Jones et al., 2015), with elevation transects at Gondola Ridge (red triangle) and Low Ridge (blue diamond), and at Mawson Glacier (Jones et al., 2020), with elevation transects at Bruce Point (purple circle) and Mt Murray (orange square). The red boundary represents the 2-D ice-flow model domain that we used in this study to investigate grounding-line migration and upstream ice thickness change. (b) The records of thinning at Mackay and Mawson Glaciers during the Holocene, with the symbols corresponding to those in (a). Rapid thinning occurred at both glaciers at ~7.5-5 Kyr ago (shown as a gray area).

sheet retreat during the Holocene (11.7-0 Kyr ago) (Crosta et al., 2018; Hillenbrand et al., 2017; Lowry et al., 2019), similar to today. In the southwestern Ross Sea (Figure 1), however, the role of the ocean and the complex bed topography in driving and controlling this retreat are not clear. The outlet glaciers persisted in a more expanded configuration than today, and possibly readvanced, in this region long after the ice sheet had retreated in the central embayment (Greenwood et al., 2018; Halberstadt et al., 2016; Lee et al., 2017). Nonlinear deglaciation of the southwestern Ross Sea then occurred—defined here as the episodic retreat (Greenwood et al., 2018; Lee et al., 2017) and abrupt increase in the thinning rate (Jones et al., 2015, Jones et al., 2020) of outlet glaciers—despite this region currently accommodating some of the coldest waters in Antarctica (Orsi & Wiederwohl, 2009; Smith et al., 2012). The spatial and temporal pattern of deglaciation has been difficult to replicate in ice sheet models, possibly because the model resolutions used are too coarse to accurately represent the complex bed topography in this region (Cuzzone et al., 2019; Lowry et al., 2019). Key questions therefore remain regarding the drivers and controls of recorded nonlinear ice-sheet behavior in the southwestern Ross Sea during the Holocene. Using regional, mesh-based ice-flow modeling that is constrained by geological data, this study aims to answer: (1) What style of ocean-driven basal melt can explain the record of deglaciation? and (2) How did bed topography control the rate and spatial pattern of retreat?

2. Ice History Constraints

The glacial history of the southwestern Ross Sea is constrained by a combination of onshore and offshore geological data (Figure 1). At the Last Glacial Maximum, ice was grounded across much of the continental shelf (Anderson et al., 2014), and the lower reaches of outlet glaciers thickened by at least 260 m relative to today (Jones et al., 2015). Landforms mapped on the seafloor reveal the nature of deglaciation. Megascale glacial lineations document the flow of Mackay and Mawson Glaciers into the southwestern Ross Sea as they retreated back to their modern configurations, while grounding-zone wedges indicate that this retreat likely occurred in the presence of an ice shelf (Greenwood et al., 2018; Lee et al., 2017). The timing of

the deglaciation is recorded at several sites. Grounded ice retreated first in the central Ross Sea, with the grounding line reaching just east of Ross Island by 8.6 Kyr ago (McKay et al., 2016) and to McMurdo Sound by ~7.5 Kyr ago (Licht et al., 1996). While the exact timing and pattern of grounding-line retreat is not accurately known, especially in the vicinity downstream of Mawson and Mackay Glaciers (Prothro et al., 2020), these data help inform when certain locations likely became free of grounded ice during the Holocene.

The main unloading of grounded ice in the southwestern Ross Sea is recorded by raised beaches dating to ~7.8 Kyr ago (Hall & Denton, 2004). This is also reflected in chronologies of outlet glacier thickness change. Rapid thinning of >200 m occurred at Mackay and Mawson Glaciers between ~7.5 and 5 Kyr ago (Jones et al., 2015; Jones et al., 2020). This event is principally recorded at ~7.5-6 Kyr ago at the sites of Gondola Ridge, Low Ridge and Bruce Point, with a possible 1-Kyr lag at the Mawson Glacier site of Mt Murray (Figure 1b). After this, both glaciers thinned by just ~15 m over ~5 Kyr during the Mid-to-Late Holocene, with a final thinning of ~25 m at Low Ridge (Mackay Glacier) to the modern glacier geometries occurring over the last ~1 Kyr (Jones et al., 2015; Jones et al., 2020; Figure 1b). The magnitude, timing and rate of this ice thinning provide key constraints on plausible scenarios of modeled outlet glacier change during the Holocene.

3. Methods

To investigate the drivers and controls of changes in past ice geometry within our study region, we used the open source finite element model Úa (Gudmundsson, 2013; Gudmundsson, 2019; Gudmundsson et al., 2012). The model solves for ice flow in the grounded and floating portions of an ice sheet simultaneously, and uses an adaptive mesh, which allows us to simulate stresses and ice thickness changes at the grounding line and where there are ice history constraints. Details of the numerical formulation can be found in the supporting information (Text S1).

3.1. Input Data and Model Setup

The model domain was designed to capture grounding-line migration and corresponding upstream ice thickness change for the period that is covered by the ice history constraints (Figure S1). A suite of ice surface and bed topography data were used to initialize our model (Text S2). To account for the potential impact of glacial isostatic adjustment on grounding-line migration (e.g., Kingslake et al., 2018) in our model simulations, we updated the bed topography through time using vertical deformation from the glacial rebound model ICE-6G, which was shown to adequately fit the relative sea level records from this region (Argus et al., 2014). We adopted the high-resolution (5.5 km) RACMO2.1/ANT model simulation (Lenaerts et al., 2012) in combination with a regional ice core derived paleo-precipitation rate (Stenni et al., 2011) to produce a spatially-variable surface mass balance (SMB) through the Holocene (Text S2). Ice shelf basal mass balance (BMB) was calculated using a depth-dependent scaling scheme, which was based on measurements of the regional vertical ocean temperature profile (Figure S2). We applied a spatially-variable BMB based on the observed temperature profile, a melt rate tuning parameter, and the ice shelf draft at each model node for each model time step (Text S2). Calving was also applied using a critical ice shelf thickness, similar to what has been applied in previous paleo-ice sheet modeling studies (e.g., Whitehouse et al., 2017), which was informed by observations of modern ice shelf thickness (Chuter & Bamber, 2015). We used the modern ice tongue thickness of Mawson and Mackay Glaciers of 150 m as the calving threshold of minimum thickness.

The model was set up in three stages (Text S3). First, we generated basal and internal conditions of regional ice flow. As sector-scale ice sheet modeling showed that ice flow in the western Ross Sea is sensitive to model parameters (e.g., enhancement factors, basal resistance, till friction angle; Lowry et al., 2020), we generated maps with low, medium and high basal slipperiness and ice rate factor values. Next, we simulated a modern ice configuration that was consistent with SMB and BMB forcings. Finally, we simulated advanced ice configurations that are approximately representative of the Early Holocene, prior to the rapid thinning episode that is recorded in the geological data; the grounding line was simulated eastward of the Southern Drygalski Trough at an area of relatively shallow bathymetry, and the glacier ice surfaces were simulated above the height of the elevation transects recording ice thickness change.
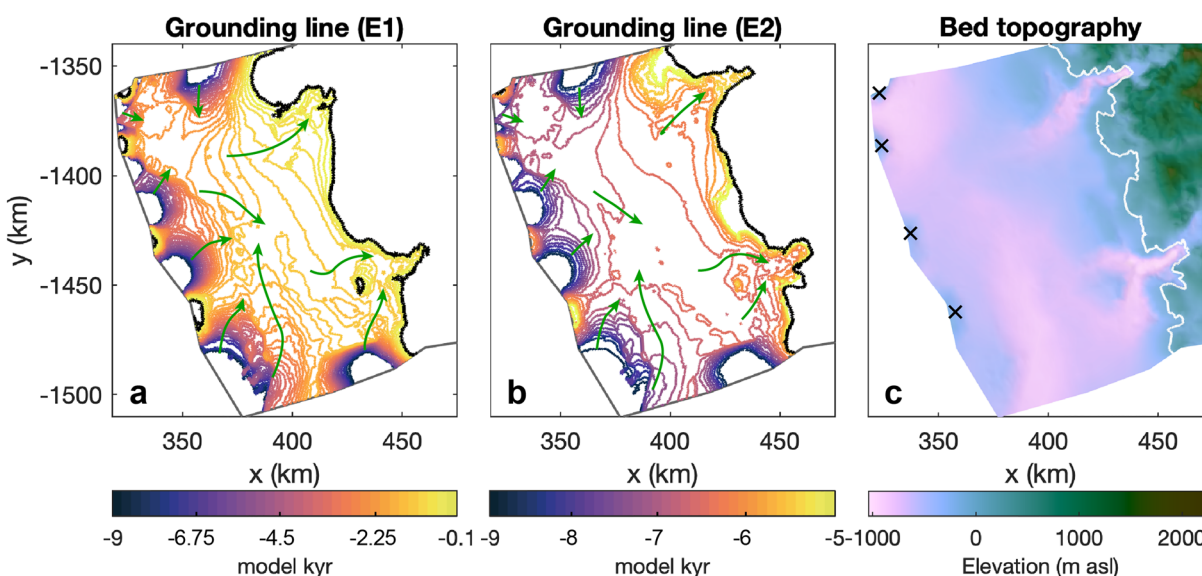
Figure 2. Simulated grounding-line retreat in the offshore region of the domain. Grounding line positions are shown in 200-year intervals for example simulations from experiments (a) E1 and (b) E2; note, grounding lines are displayed for 9-0 model Kyr ago for E1 and 9-5 model Kyr ago for E2. A bold black line denotes the final position at 0 model Kyr, while green schematic arrows highlight retreat directions. Grounding-line positions are plotted for all simulations in Figure S4. (c) Bed topography in the lower reaches of the model domain, with the observed modern grounding line highlighted in white and pinning points as crosses. Retreat is faster in regions of deeper topography in both experiments; however, the retreat rate is much lower in experiment E1. The final grounding-line position (at 0 model Kyr ago) does not reach the present-day position in E1, but does in E2, also implying that a more enhanced ocean thermal forcing was needed during the Holocene to reach the modern ice configuration.

3.2. Model Experiments

We conducted a series of time-dependent experiments to investigate the potential oceanic drivers and controls of grounding-line migration and upstream glacier thinning (Text S4). As the timing and relative magnitude of ocean thermal forcing in the Ross Sea during the Holocene remains unknown, we tested whether a linear time-dependent (E1) or enhanced Early-to-Mid Holocene (E2) ocean thermal forcing could cause accelerated grounding-line retreat and glacier thinning. For E1, we decreased the BMB (i.e., increased the ice shelf melt rate) linearly using the melt rate tuning parameter from the advanced configuration values to the present-day values for 9-0 model Kyr ago. For E2, we decreased the BMB linearly from its advanced configuration values to the present-day values for 9-6 model Kyr ago, and then maintained constant BMB values until 0 model Kyr. Two additional experiments aimed to: test whether a 100-year period of enhanced ocean thermal forcing, similar to that recorded elsewhere in Antarctica during the Holocene (e.g., Etourneau et al., 2013), is able to produce the recorded rapid glacier thinning in the Mid Holocene (E3); and, replicate the pattern of ice surface lowering recorded in the Mid-to-Late Holocene (E4) (Text S4).

For each experiment, simulations were carried out using different combinations of the basal slipperiness and ice rate factor maps to account for the uncertainty in these parameters. The same time-varying changes in glacial isostatic adjustment and precipitation between 9 and 0 Kyr ago were used in all experiments. The results of the experiments were then evaluated based on agreement with the geological data that constrain the timings of ice surface lowering at Mackay and Mawson Glaciers.

4. Results

4.1. Pattern of Grounding-Line Retreat in the Southwestern Ross Sea

The spatial and temporal pattern of grounding-line migration provides an indication of the sensitivity of this portion of the ice sheet to ocean forcing during deglaciation. The spatial pattern of retreat is similar between experiments, in all of the simulations (Figures 2 and S4). The grounding line initially remains pinned to the topographic high points that extend north from Ross Island (0–225 m bsl), along the simulated advanced ice front, with retreat occurring in the areas of deeper bathymetry between the high points (>550–900 m bsl).
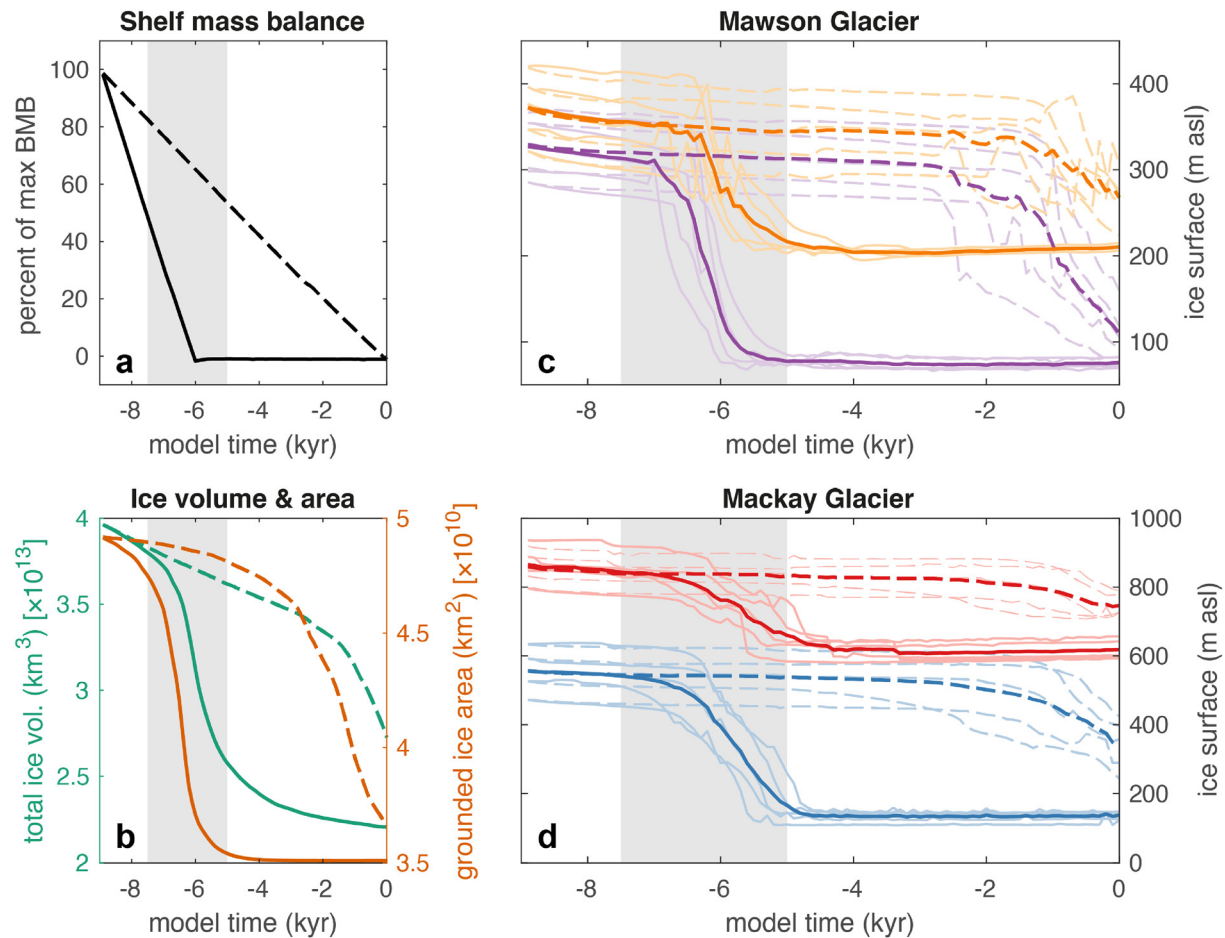
Figure 3. (a) Basal mass balance (BMB) forcing in experiments E1 (dashed line) and E2 (solid line), with the resulting simulated changes in ice volume and grounded ice area (b), and corresponding changes in ice surface elevation at (c) Mawson Glacier and (d) Mackay Glacier. The sites of Mt Murray, Bruce Point, Gondola Ridge and Low Ridge are colored orange, purple, red and blue, respectively. The bold lines represent the mean of the individual simulations in each experiment, while the period of observed rapid thinning (7.5-5 Kyr ago) is highlighted as a gray area. Accelerated ice loss occurs in both E1 and E2, however, only E2 replicates the timing recorded by the geological data.

This is the case for experiments E1 and E2, despite the abrupt decrease in BMB (i.e., increase in melt rate) applied in E2. Retreat then accelerates once the grounding line moves inland of these topographic highs. The direction of this retreat is broadly along troughs and up onto shallower banks, similar to that indicated by seafloor landforms (Figure 2). Notably, the grounding line retreats back toward Mackay Glacier from the area just north of McMurdo Sound and across the southern end of the Southern Drygalski Trough, and retreats both northward and southward in the Southern Drygalski Tough downstream of Mawson Glacier. The rate of retreat decreases slightly once the grounding line reaches the mouths of Mawson and Mackay Glaciers, where the bathymetry is deep but the glaciers are embayed in narrow fjords. Together, these experiments highlight that the pattern of retreat is controlled by the bed topography and lateral geometry, with accelerated ice loss occurring following retreat of the grounding line through overdeepened basins after the grounding line detached from local topographic highs.

4.2. Inland Ice Loss During the Holocene

Rapid ice volume loss and ice surface lowering accompanies the period of accelerated grounding-line retreat in all simulations despite the different style of ice shelf mass balance forcing that is applied (Figure 3). However, using a linear decrease in BMB at 9-0 model Kyr ago (E1) fails to reproduce the timing of the recorded rapid thinning event, and this finding is not affected by particular parameter values (slipperiness and ice rate factor). An accelerated decrease in the area of grounded ice only occurs from ~2 model Kyr ago,

with abrupt ice volume loss and corresponding ice surface lowering at the Mawson and Mackay Glacier sites occurring from ~1 model Kyr ago (Figure 3), which is a significant mismatch with the geological data.

An enhanced decrease in BMB (i.e., increase in the sub-shelf melt rate) at 9-6 model Kyr ago (E2) is required to match the timing of recorded rapid thinning in the Mid Holocene (Figure 3). In these simulations, ~100–400 m of ice surface lowering is simulated at Mawson and Mackay Glacier, which is of a relatively smaller magnitude at the more upstream site at each glacier. Notably, a dynamic adjustment of the ice surface at Mawson Glacier's upstream site (Mt Murray) occurs in all of the E2 simulations. This causes the end of the accelerated thinning to be delayed by up to ~1 Kyr relative to the downstream site (Bruce Point), replicating what was recorded by the geological data (Figure 1b). The rates of rapid thinning simulated in experiment E2 also broadly match the rates estimated from the geological data (Figure S5). Importantly, clear differences in the timing of the simulated rapid thinning exist between experiments E1 and E2. Prescribing a 100-year peak in ice shelf melt at the onset of recorded rapid thinning (E3) produces only a temporary reduction in ice volume, and minor and/or temporary ice surface lowering at Mawson and Mackay Glaciers (Figure S6). These experiments therefore support sustained, enhanced ice shelf melt at 9-6 model Kyr ago as the main driver of Mid-Holocene ice loss.

Observations show that ice loss continued at Mawson and Mackay Glaciers into the Late Holocene, with a second phase of accelerated ice thinning recorded at one site (Figure 1b). This pattern of Mid-to-Late Holocene thinning is not captured in any of the simulations in experiments E1 and E2 (Figure 3). Instead, the recorded gradual thinning at Gondola Ridge (Mackay) and Mt Murray (Mawson), with a Late Holocene episode of accelerated thinning at Low Ridge (Mackay), can be broadly replicated when a small-magnitude gradual decrease in BMB is applied at 6–0 model Kyr ago (E4) (Figure S7). At Low Ridge, this second phase of accelerated thinning occurs when the grounding line reaches the deepest part of the trough.

5. Discussion

5.1. Control of Bed Topography on Deglaciation

Our use of regional-scale finite element modeling with unstructured grids has enabled us to capture complex outlet glacier retreat patterns, which has not been possible using continental-scale and sector-scale uniform-grid ice sheet models (Cuzzone et al., 2019; Lowry et al., 2019). The simulations show that shallow banks and seamounts—including features <10 km wide—provided critical pinning points during deglaciation, while deeper beds allowed for accelerated grounding-line retreat, supporting interpretations of seafloor landforms (Greenwood et al., 2018; Halberstadt et al., 2016). A reorganization of ice flow with two opposing non-contemporaneous flow events during retreat has been proposed for this region, based on the direction of megascale glacial lineations in the Southern Drygalski Trough (Greenwood et al., 2018). However, we show that these apparent opposing flow directions could be possible from divergent ice flow downstream of Mawson Glacier during retreat, where ice preferentially flowed toward the deeper bathymetry. As deglaciation progressed, simulated grounding-line retreat onto banks produced isolated pockets and narrow zones of grounded ice, consistent with the idea that ice became afloat in deeper areas while still being grounded on either side of the troughs (Greenwood et al., 2018).

The Holocene deglaciation of the southwestern Ross Sea illustrates how bed topography can exert a fundamental control on grounding-line migration. In particular, the rate of grounding-line retreat is shown to be limited by shallow-bed pinning points, even when enhanced ice shelf melt rates are applied. Increased basal drag at pinning points can slow adjacent ice velocities, increasing ice volume and lateral friction, which can potentially lead to grounding-line advance (Favier et al., 2012; Goldberg et al., 2009). Progressive thinning of the ice at these pinning points eventually leads to floatation and retreat of the grounding line, which accelerates following detachment from this shallow bed topography (Figure 2). Our simulations support the idea that a critical bathymetric threshold may exist under sustained forcing where retreat into deeper areas (>~230 m deep in the southwestern Ross Sea) leads to massively increased ice discharge and rapid retreat (Favier et al., 2012; Gasson et al., 2015). The modeling indicates that retreat and associated ice surface drawdown accelerated during the Holocene until ice thickness at the grounding line reduced on an upward-sloping bed (Schoof, 2007) and/or the lateral drag was increased by narrowing of troughs (Jamieson et al., 2014) at the mouths of the outlet glaciers. Ice sheet modeling has shown that bed topography

controls the onset and pattern of grounding-line retreat observed over recent decades, and likely into the future (Favier et al., 2016; Seroussi et al., 2017). Using an example of ice sheet retreat from the geological past, this work shows that bed topography plays a similar role on multi-centennial timescales, and highlights the importance of suitably constraining kilometer-scale bed topography for accurate simulations of grounding-line migration.

5.2. Ocean Thermal Forcing During the Holocene

Our experiments have demonstrated that a sustained period of enhanced sub-ice shelf melt during the Early-to-Mid Holocene is required to initiate retreat from stable pinning points and cause rapid thinning of the outlet glaciers to occur in the Mid Holocene.

There are three different modes by which the ocean can melt an ice shelf and potentially initiate grounding-line retreat (Jacobs et al., 1992). The first mode is characterized by relatively cold and dense waters, and is how ice shelf melt in the western Ross Sea is regulated today; High Salinity Shelf Water (HSSW) is formed from brine rejection during sea-ice production in the Ross Sea Polynya (Jendersie et al., 2018; Orsi & Wiederwohl, 2009). A second mode results from the atmospheric warming of surface waters during summer months, with ice shelf melt limited to the near-surface and calving front (Stewart et al., 2019). The final mode involves the incursion of relatively warm modified Circumpolar Deep Water (mCDW), which is responsible for the highest ice shelf melt rates observed in Antarctica today (Adusumilli et al., 2020). In the absence of cold water gyres and HSSW, mCDW is able to spread across the continental shelf and reach ice shelf cavities, causing substantial sub-shelf melt to occur near the grounding line (Jacobs et al., 1992; Silvano et al., 2016). While all modes of ice shelf melt could have contributed to grounding-line retreat in the western Ross Sea during the Holocene, warm mCDW has the greatest potential for causing a sustained period of enhanced sub-shelf melt in the Early-to-Mid Holocene.

Modified CDW is not observed in the southwestern Ross Sea today, however, proxy-based evidence indicates that oceanic conditions were different during the Holocene. A more southerly position of the Southern Hemisphere westerly wind belt drove an increased incursion of mCDW between 10.4 and 7.5 Kyr ago in the Amundsen Sea region (Hillenbrand et al., 2017). A similar inflow of mCDW could also have been possible in the Ross Sea at this time, as a large Ross Ice Shelf cavity had possibly not yet developed (Lowry et al., 2019), meaning that the production of sea ice and resulting HSSW was not yet occurring (Ashley et al., 2021) and thus not able to block mCDW (Jacobs et al., 1992). A freshening of the Southern Ocean during deglaciation could also have led to reduced Antarctic Bottom Water formation and then incursions of mCDW onto the Ross Sea continental shelf during the Early Holocene (Golledge et al., 2014). Modern oceanic conditions in the Ross Sea were then likely reached by the Mid-to-Late Holocene (Ashley et al., 2021), with ice shelf melt rates and resulting variability of outlet glacier grounding-line positions possibly regulated by changes in the efficiency of the Ross Sea Polynya (Mezgec et al., 2017) and the summer warming of surface waters (Crosta et al., 2018).

The recorded timing and magnitude of Holocene ice loss that was simulated in this study is not unique to the southwestern Ross Sea. Accelerated thinning during the Early-to-Mid Holocene and ice margin variability from the Mid-to-Late Holocene is documented across Antarctica (Hall, 2009; Small et al., 2019). The broad synchronicity suggests that a circum-Antarctic flux of mCDW occurred during the Holocene, driving grounding-line retreat and rapid ice sheet thinning at a number of sites.

6. Conclusions

We applied ice-flow modeling in combination with geological data to investigate the controls and drivers of ice margin retreat during the Holocene. The use of a regional, mesh-based model allowed us to capture complex grounding-line dynamics associated with km-scale bed topography. In particular, the modeling highlights the importance of pinning points in controlling retreat rates, and supports the idea that retreat beyond a bathymetric threshold can lead to accelerated retreat and ice surface drawdown. While bed topography exerts a strong control on grounding-line position, the observed ice loss cannot be explained solely by self-sustained unstable retreat. Enhanced ocean-driven melt during the Early-to-Mid Holocene (9-6 Kyr ago) was required to replicate the timing of rapid ice thinning recorded in the Mid Holocene (7.5-5 Kyr ago)

in the southwestern Ross Sea. Available evidence supports incursions of mCDW as the most likely mechanism that drove sub-shelf melt and grounding-line retreat during the Early-to-Mid Holocene, with later changes possibly regulated by the Ross Sea Polynya and seasonal ocean surface warming. The processes that will dictate future Antarctic ice sheet mass loss remain uncertain, and this work demonstrates that ocean temperature and bed topography act together to both regulate and enhance the amount and rate of nonlinear ice loss on timescales relevant to the coming centuries.

Data Availability Statement

The model used in this study (Úa) is available from Gudmundsson (2019; https://doi.org/10.5281/zenodo.3706624), while the geological data used are archived at ICE-D (http://antarctica.ice-d.org/) and described in Jones et al. (2015) and Jones et al. (2020). The model output can be made available upon request.

References

Adusumilli, S., Fricker, H. A., Medley, B., Padman, L., & Siegfried, M. R. (2020). Interannual variations in meltwater input to the Southern Ocean from Antarctic ice shelves. *Nature Geoscience*, *13*, 616–620. https://doi.org/10.1038/s41561-020-0616-z

Anderson, J. B., Conway, H., Bart, P. J., Witus, A. E., Greenwood, S. L., McKay, R. M., et al. (2014). Ross Sea paleo-ice sheet drainage and deglacial history during and since the LGM. *Quaternary Science Reviews*, *100*, 31–54. https://doi.org/10.1016/j.quascirev.2013.08.020

Argus, D. F., Peltier, W. R., Drummond, R., & Moore, A. W. (2014). The Antarctica component of postglacial rebound model ICE-6G_C (VM5a) based on GPS positioning, exposure age dating of ice thicknesses, and relative sea level histories. *Geophysical Journal International*, *198*(1), 537–563. https://doi.org/10.1093/gji/ggu140

Arndt, J. E., Schenke, H. W., Jakobsson, M., Nitsche, F. O., Buys, G., Goleby, B., et al. (2013). The International Bathymetric Chart of the Southern Ocean (IBCSO) Version 1.0 – A new bathymetric compilation covering circum-Antarctic waters. *Geophysical Research Letters*, *40*(12), 3111–3117. https://doi.org/10.1002/grl.50413

Ashley, K. E., Bendle, J. A., McKay, R., Etourneau, J., Jimenez-Espejo, F. J., Condron, A., et al. (2021). Mid-Holocene Antarctic sea-ice increase driven by marine ice sheet retreat. *Climate of the Past*, *17*, 1–19. https://doi.org/10.5194/cp-17-1-2021

Baroni, C., & Hall, B. L. (2004). A new Holocene relative sea-level curve for Terra Nova Bay, Victoria Land, Antarctica. *Journal of Quaternary Science*, *19*(4), 377–396. https://doi.org/10.1002/jqs.825

Chuter, S., & Bamber, J. (2015). Antarctic ice shelf thickness from CryoSat-2 radar altimetry. *Geophysical Research Letters*, *42*(24), 10721–10729. https://doi.org/10.1002/2015GL066515

Crosta, X., Crespin, J., Swingedouw, D., Marti, O., Masson-Delmotte, V., Etourneau, J., et al. (2018). Ocean as the main driver of Antarctic ice sheet retreat during the Holocene. *Global and Planetary Change*, *166*, 62–74. https://doi.org/10.1016/j.gloplacha.2018.04.007

Cuzzone, J. K., Larour, E., Briner, J. P., & Lambert, C. (2019). The impact of model resolution on the simulated Holocene retreat of the southwestern Greenland ice sheet using the Ice Sheet System Model (ISSM). *The Cryosphere*, *13*(3), 879–893. https://doi.org/10.5194/tc-2018-249

DeConto, R. M., & Pollard, D. (2016). Contribution of Antarctica to past and future sea-level rise. *Nature*, *531*(7596), 591–597. https://doi.org/10.1038/nature17145

Etourneau, J., Collins, L., Willmott, V., Kim, J.-H., Barbara, L., Leventer, A., et al. (2013). Holocene climate variations in the western Antarctic Peninsula: Evidence for sea ice extent predominantly controlled by changes in insolation and ENSO variability. *Climate of the Past*, *9*(4), 1431–1446. https://doi.org/10.5194/CP-9-1431-2013

Favier, L., Gagliardini, O., Durand, G., & Zwinger, T. (2012). A three-dimensional full Stokes model of the grounding line dynamics: Effect of a pinning point beneath the ice shelf. *The Cryosphere Discussions*, *5*, 1995–2033. https://doi.org/10.5194/tcd-5-1995-2011

Favier, L., Pattyn, F., Berger, S., & Drews, R. (2016). Dynamic influence of pinning points on marine ice-sheet stability: A numerical study in Dronning Maud Land, East Antarctica. *The Cryosphere*, *10*, 2623–2635. https://doi.org/10.5194/tc-10-2623-2016

Gasson, E., DeConto, R., & Pollard, D. (2015). Antarctic bedrock topography uncertainty and ice sheet stability. *Geophysical Research Letters*, *42*(13), 5372–5377. https://doi.org/10.1002/2015GL064322

Goldberg, D., Holland, D., & Schoof, C. (2009). Grounding line movement and ice shelf buttressing in marine ice sheets. *Journal of Geophysical Research*, *114*, F04026. https://doi.org/10.1029/2008JF001227

Golledge, N. R., Kowalewski, D. E., Naish, T. R., Levy, R. H., Fogwill, C. J., & Gasson, E. G. (2015). The multi-millennial Antarctic commitment to future sea-level rise. *Nature*, *526*(7573), 421. https://doi.org/10.1038/nature15706

Golledge, N. R., Menviel, L., Carter, L., Fogwill, C. J., England, M. H., Cortese, G., & Levy, R. H. (2014). Antarctic contribution to meltwater pulse 1A from reduced Southern Ocean overturning. *Nature Communications*, *5*, 5107. https://doi.org/10.1038/ncomms6107

Greenwood, S. L., Simkins, L. M., Halberstadt, A. R. W., Prothro, L. O., & Anderson, J. B. (2018). Holocene reconfiguration and readvance of the East Antarctic Ice Sheet. *Nature Communications*, *9*, 3176. https://doi.org/10.1038/s41467-018-05625-3

Gudmundsson, G. (2013). Ice-shelf buttressing and the stability of marine ice sheets. *The Cryosphere*, *7*(2), 647–655. https://doi.org/10.5194/tc-7-647-2013

Gudmundsson, G., Krug, J., Durand, G., Favier, L., & Gagliardini, O. (2012). The stability of grounding lines on retrograde slopes. *The Cryosphere*, *6*, 1497–1505. https://doi.org/10.5194/tc-6-1497-2012

Gudmundsson, G. H. (2019). *UaSource, Version v2019b*. Zenodo. https://doi.org/10.5281/zenodo.3706624

Gudmundsson, G. H., Paolo, F. S., Adusumilli, S., & Fricker, H. A. (2019). Instantaneous Antarctic ice sheet mass loss driven by thinning ice shelves. *Geophysical Research Letters*, *46*(23), 13903–13909. https://doi.org/10.1029/2019GL085027

Halberstadt, A. R. W., Simkins, L. M., Greenwood, S. L., & Anderson, J. B. (2016). Past ice-sheet behavior: Retreat scenarios and changing controls in the Ross Sea, Antarctica. *The Cryosphere*, *10*, 1003–1020. https://doi.org/10.5194/tc-10-1003-2016

Hall, B. L. (2009). Holocene glacial history of Antarctica and the sub-Antarctic islands. *Quaternary Science Reviews*, *28*(21–22), 2213–2230. https://doi.org/10.1016/j.quascirev.2009.06.011

Hall, C. B., & Denton, G. H. (2004). Holocene relative sea-level history of the Southern Victoria Land Coast, Antarctica. *Global and Planetary Change*, *42*(1), 241–263. https://doi.org/10.1016/j.gloplacha.2003.09.004

Hillenbrand, C.-D., Smith, J. A., Hodell, D. A., Greaves, M., Poole, C. R., Kender, S., et al. (2017). West Antarctic Ice Sheet retreat driven by Holocene warm water incursions. *Nature*, *547*(7661), 43–48. https://doi.org/10.1038/nature22995

Howat, I. M., Porter, C., Smith, B. E., Noh, M.-J., & Morin, P. (2019). The Reference Elevation Model of Antarctica. *The Cryosphere*, *13*(2), 665–674. https://doi.org/10.5194/tc-13-665-2019

Jacobs, S., Helmer, H., Doake, C., Jenkins, A., & Frolich, R. (1992). Melting of ice shelves and the mass balance of Antarctica. *Journal of Glaciology*, *38*(130), 375–387. https://doi.org/10.3189/S0022143000002252

Jamieson, S. S. R., Vieli, A., Cofaigh, C. Ó., Stokes, C. R., Livingstone, S. J., & Hillenbrand, C.-D. (2014). Understanding controls on rapid ice-stream retreat during the last deglaciation of Marguerite Bay, Antarctica, using a numerical model. *Journal of Geophysical Research: Earth Surface*, *119*(2), 247–263. https://doi.org/10.1002/2013JF002934

Jendersie, S., Williams, M. J., Langhorne, P. J., & Robertson, R. (2018). The density-driven winter intensification of the Ross Sea circulation. *Journal of Geophysical Research: Oceans*, *123*(11), 7702–7724. https://doi.org/10.1029/2018JC013965

Jones, R., Mackintosh, A., Norton, K. P., Golledge, N. R., Fogwill, C., Kubík, P. W., et al. (2015). Rapid Holocene thinning of an East Antarctic outlet glacier driven by marine ice sheet instability. *Nature Communications*, *6*, 8910. https://doi.org/10.1038/ncomms9910

Jones, R. S., Whitmore, R. J., Mackintosh, A. N., Norton, K. P., Eaves, S. R., Stutz, J., & Christl, M. (2020). Regional-scale abrupt Mid-Holocene ice sheet thinning in the western Ross Sea, Antarctica. *Geology*, *49*, 3.

Kingslake, J., Scherer, R., Albrecht, T., Coenen, J., Powell, R., Reese, R., et al. (2018). Extensive retreat and re-advance of the West Antarctic ice sheet during the Holocene. *Nature*, *558*(7710), 430. https://doi.org/10.1038/s41586-018-0208-x

Konrad, H., Shepherd, A., Gilbert, L., Hogg, A. E., McMillan, M., Muir, A., & Slater, T. (2018). Net retreat of Antarctic glacier grounding lines. *Nature Geoscience*, *11*(4), 258. https://doi.org/10.1038/s41561-018-0082-z

Lee, J. I., McKay, R. M., Golledge, N. R., Yoon, H. I., Yoo, K.-C., Kim, H. J., & Hong, J. K. (2017). Widespread persistence of expanded East Antarctic glaciers in the southwest Ross Sea during the last deglaciation. *Geology*, *45*(5), 403–406. https://doi.org/10.1130/G38715.1

Lenaerts, J. T. M., Van Den Broeke, M. R., Scarchilli, C., & Agosta, C. (2012). Impact of model resolution on simulated wind, drifting snow and surface mass balance in Terre Adélie, East Antarctica. *Journal of Glaciology*, *58*(211), 821–829. https://doi.org/10.3189/2012JoG12J020

Licht, K. J., Jennings, A. E., Andrews, J. T., & Williams, K. M. (1996). Chronology of late Wisconsin ice retreat from the western Ross Sea, Antarctica. *Geology*, *24*(3), 223–226. https://doi.org/10.1130/0091-7613(1996)024%3C0223:COLWIR%3E2.3.CO;2

Lowry, D. P., Golledge, N. R., Bertler, N. A., Jones, R. S., & McKay, R. (2019). Deglacial grounding-line retreat in the Ross Embayment, Antarctica, controlled by ocean and atmosphere forcing. *Science Advances*, *5*(8), eaav8754. https://doi.org/10.1126/sciadv.aav8754

Lowry, D. P., Golledge, N. R., Bertler, N. A., Jones, R. S., McKay, R., & Stutz, J. (2020). Geologic controls on ice sheet sensitivity to deglacial climate forcing in the Ross Embayment, Antarctica. *Quaternary Science Advances*, *1*, 100002. https://doi.org/10.1016/j.qsa.2020.100002

McKay, R., Golledge, N. R., Maas, S., Naish, T., Levy, R., Dunbar, G., & Kuhn, G. (2016). Antarctic marine ice-sheet retreat in the Ross Sea during the early Holocene. *Geology*, *44*(1), 7–10. https://doi.org/10.1130/G37315.1

McMillan, M., Shepherd, A., Sundal, A., Briggs, K., Muir, A., Ridout, A., et al. (2014). Increased ice losses from Antarctica detected by CryoSat-2. *Geophysical Research Letters*, *41*(11), 3899–3905. https://doi.org/10.1002/2014GL060111

Meredith, M., Sommerkorn, M., Cassotta, S., Derksen, C., Ekaykin, A., Hollowed, A., et al. (2019). Polar regions. In H. O. Pörtner, et al., (Eds.), *IPCC Special Report on the Ocean and Cryosphere in a Changing Climate* (pp. 203–320).

Mezgec, K., Stenni, B., Crosta, X., Masson-Delmotte, V., Baroni, C., Braida, M., et al. (2017). Holocene sea ice variability driven by wind and polynya efficiency in the Ross Sea. *Nature Communications*, *8*(1), 1334. https://doi.org/10.1038/s41467-017-01455-x

Noble, T., Rohling, E., Aitken, A. R. A., Bostock, H. C., Chase, Z., Gomez, N., et al. (2020). The sensitivity of the Antarctic Ice Sheet to a changing climate: Past, present, and future. *Reviews of Geophysics*, *58*(4), e2019RG000663. https://doi.org/10.1029/2019RG000663

Oppenheimer, M., Glavovic, B. C., Hinkel, J., van de Wal, R., Magnan, A. K., et al. (2019). Sea level rise and implications for low-lying islands, coasts and communities. In H. O. Pörtner, et al., (Eds.), *IPCC Special Report on the Ocean and Cryosphere in a Changing Climate*.

Orsi, A. H., & Wiederwohl, C. L. (2009). A recount of Ross Sea waters. *Deep Sea Research Part II*, *56*(13–14), 778–795. https://doi.org/10.1016/j.dsr2.2008.10.033

Prothro, L. O., Majewski, W., Yokoyama, Y., Simkins, L. M., Anderson, J. B., Yamane, M., et al. (2020). Timing and pathways of East Antarctic Ice Sheet retreat. *Quaternary Science Reviews*, *230*, 106166. https://doi.org/10.1016/j.quascirev.2020.106166

Rignot, E., Jacobs, S., Mouginot, J., & Scheuchl, B. (2013). Ice-shelf melting around Antarctica. *Science*, *341*(6143), 266–270. https://doi.org/10.1126/science.1235798

Rignot, E., Mouginot, J., Scheuchl, B., van den Broeke, M., van Wessem, M. J., & Morlighem, M. (2019). Four decades of Antarctic Ice Sheet mass balance from 1979–2017. *Proceedings of the National Academy of Sciences of the United States of America*, *116*(4), 1095–1103. https://doi.org/10.1073/pnas.1812883116

Schoof, C. (2007). Ice sheet grounding line dynamics: Steady states, stability, and hysteresis. *Journal of Geophysical Research*, *112*, F03S28. https://doi.org/10.1029/2006JF000664

Seroussi, H., Nakayama, Y., Larour, E., Menemenlis, D., Morlighem, M., Rignot, E., & Khazendar, A. (2017). Continued retreat of Thwaites Glacier, West Antarctica, controlled by bed topography and ocean circulation. *Geophysical Research Letters*, *44*(12), 6191–6199. https://doi.org/10.1002/2017GL072910

Shepherd, A., Ivins, E., Rignot, E., Smith, B., van den Broeke, M., Velicogna, I., et al. (2018). Mass balance of the Antarctic Ice Sheet from 1992 to 2017. *Nature*, *556*, 219–222. https://doi.org/10.1038/s41586-018-0179-y

Silvano, A., Rintoul, S. R., & Herraiz-Borreguero, L. (2016). Ocean-ice shelf interaction in East Antarctica. *Oceanography*, *29*(4), 130–143. https://doi.org/10.5670/oceanog.2016.105

Small, D., Bentley, M. J., Jones, R. S., Pittard, M. L., & Whitehouse, P. L. (2019). Antarctic ice sheet palaeo-thinning rates from vertical transects of cosmogenic exposure ages. *Quaternary Science Reviews*, *206*, 65–80. https://doi.org/10.1016/j.quascirev.2018.12.024

Smith, B., Fricker, H. A., Gardner, A. S., Medley, B., Nilsson, J., Paolo, F. S., et al. (2020). Pervasive ice sheet mass loss reflects competing ocean and atmosphere processes. *Science*, *368*(6496), 1239–1242. https://doi.org/10.1126/science.aaz5845

Smith, W., Sedwick, P., Arrigo, K., Ainley, D., & Orsi, A. (2012). The Ross Sea in a sea of change. *Oceanography*, *25*(3), 90–103. https://doi.org/10.5670/oceanog.2012.80

Stenni, B., Buiron, D., Frezzotti, M., Albani, S., Barbante, C., Bard, E., et al. (2011). Expression of the bipolar see-saw in Antarctic climate records during the last deglaciation. *Nature Geoscience*, *4*(1), 46–49. https://doi.org/10.1038/ngeo1026

Stewart, C. L., Christoffersen, P., Nicholls, K. W., Williams, M. J., & Dowdeswell, J. A. (2019). Basal melting of Ross Ice Shelf from solar heat absorption in an ice-front polynya. *Nature Geoscience*, *12*(6), 435. https://doi.org/10.1038/s41561-019-0356-0

Tigchelaar, M., Timmermann, A., Friedrich, T., Heinemann, M., & Pollard, D. (2019). Nonlinear response of the Antarctic Ice Sheet to late Quaternary sea level and climate forcing. *The Cryosphere*, *13*(10), 2615–2631. https://doi.org/10.5194/tc-13-2615-2019

Whitehouse, P. L., Bentley, M. J., Vieli, A., Jamieson, S. S., Hein, A. S., & Sugden, D. E. (2017). Controls on last glacial maximum ice extent in the Weddell Sea embayment, Antarctica. *Journal of Geophysical Research: Earth Surface*, *122*(1), 371–397. https://doi.org/10.1002/2016JF004121

References From the Supporting Information

Alley, R. B., Blankenship, D., Bentley, C. R., & Rooney, S. (1987). Till beneath ice stream B: 3. Till deformation: Evidence and implications. *Journal of Geophysical Research*, *92*(B9), 8921–8929. https://doi.org/10.1029/JB092iB09p08921

Bereiter, B., Shackleton, S., Baggenstos, D., Kawamura, K., & Severinghaus, J. (2018). Mean global ocean temperatures during the last glacial transition. *Nature*, *553*(7686), 39. https://doi.org/10.1038/nature25152

De Rydt, J., Gudmundsson, G., Rott, H., & Bamber, J. (2015). Modeling the instantaneous response of glaciers after the collapse of the Larsen B Ice Shelf. *Geophysical Research Letters*, *42*(13), 5355–5363. https://doi.org/10.1002/2015GL064355

Engwirda, D. (2014). *Locally optimal delaunay-refinement and optimisation-based mesh generation* (PhD thesis). The University of Sydney.

Fretwell, P., Pritchard, H. D., Vaughan, D. G., Bamber, J., Barrand, N., Bell, R., et al. (2013). Bedmap2: Improved ice bed, surface and thickness datasets for Antarctica. *The Cryosphere*, *7*(1), 375–393. https://doi.org/10.5194/tc-7-375-2013

Kim, J. H., Crosta, X., Willmott, V., Renssen, H., Bonnin, J., Helmke, P., et al. (2012). Holocene subsurface temperature variability in the eastern Antarctic continental margin. *Geophysical Research Letters*, *39*, L06705. https://doi.org/10.1029/2012GL051157

Kobashi, T., Menviel, L., Jeltsch-Thömmes, A., Vinther, B. M., Box, J. E., Muscheler, R., et al. (2017). Volcanic influence on centennial to millennial Holocene Greenland temperature change. *Scientific Reports*, *7*(1), 1441. https://doi.org/10.1038/s41598-017-01451-7

Liu, Z., Otto-Bliesner, B. L., He, F., Brady, E. C., Thomas, R., Clark, P. U., et al. (2009). Transient simulation of last deglaciation with a new mechanism for Bølling-Allerød warming. *Science*, *325*(5938), 310–314. https://doi.org/10.1126/science.1171041

MacAyeal, D. R. (1989). Large-scale ice flow over a viscous basal sediment: Theory and application to ice stream B, Antarctica. *Journal of Geophysical Research*, *94*(B4), 4071–4087. https://doi.org/10.1029/JB094iB04p04071

Pahnke, K., & Sachs, J. (2006). Sea surface temperatures of southern midlatitudes 0–160 kyr B.P. *Paleoceanography*, *21*, PA2003. https://doi.org/10.1029/2005PA001191

Reese, R., Albrecht, T., Mengel, M., Asay-Davis, X., & Winkelmann, R. (2018). Antarctic sub-shelf melt rates via PICO. *The Cryosphere*, *12*(6), 1969–1985. https://doi.org/10.5194/tc-12-1969-2018

Reese, R., Gudmundsson, G. H., Levermann, A., & Winkelmann, R. (2018). The far reach of ice-shelf thinning in Antarctica. *Nature Climate Change*, *8*(1), 53. https://doi.org/10.1038/s41558-017-0020-x

Shevenell, A. E., Ingalls, A. E., Domack, E. W., & Kelly, C. (2011). Holocene Southern Ocean surface temperature variability west of the Antarctic Peninsula. *Nature*, *470*(7333), 250–254. https://doi.org/10.1038/nature09751